PAPER • **OPEN ACCESS**

MHD peristaltic flow of a hyperbolic tangent fluid in a non-uniform channel with heat and mass transfer

To cite this article: R Saravana *et al* 2017 *IOP Conf. Ser.: Mater. Sci. Eng.* **263** 062006

View the article online for updates and enhancements.

Related content

- Peristaltic flow and heat transfer of a Herschel-Bulkley fluid in an inclined non-uniform channel with wall properties
G Sucharitha, K Vajravelu, S Sreenadh et al.
- Magnetic field effects on peristaltic flow of blood in a non-uniform channel
R Latha and B Rushi Kumar
- Slip effects on streamline topologies and their bifurcations for peristaltic flows of a viscous fluid
Z. Asghar and N. Ali

This content was downloaded from IP address 191.180.157.129 on 05/02/2018 at 02:57

IOP Conf. Series: Materials Science and Engineering **263** (2017) 062006 doi:10.1088/1757-899X/263/6/062006

MHD peristaltic flow of a hyperbolic tangent fluid in a non-uniform channel with heat and mass transfer

R Saravana[1], R Hemadri Reddy[2], J Suresh Goud[2] and S Sreenadh[3]
[1]Department of Mathematics, Madanapalle Institute of Technology and Science, Madanapalle 517 325, India
[2]Department of Mathematics, School of Advanced Science, VIT University, Vellore 632 014, India
[3]Department of Mathematics, Sri Venkateswara University, Tirupati 517 502, India

E-mail: saravanasvu@gmail.com

Abstract. The influence of elastic wall properties on the peristaltic transport of a conducting hyperbolic tangent fluid in a non-uniform channel is investigated with heat and mass transfer. The flow is examined in a fixed frame of reference under the assumptions of long wavelength and low Reynolds number. The velocity slip, temperature and concentration jump boundary conditions are considered at the walls. The perturbation method of solution for stream function, velocity, temperature, concentration and the coefficient of heat transfer are obtained in terms of small Weissenberg number. The influence of several pertinent parameters on the flow are discussed by plotting graphs. The trapping phenomenon is also analysed. It is noticed that the size of the trapping bolus increases with increasing the power law index of hyperbolic tangent fluid.

Nomenclature

a	wave amplitude (m)	u , v	Distribution of velocity in flow direction and perpendicular directions respectively (m/s)
B_0	magnetic field strength (T)	We	Weissenberg number
C	Dimensional concentration (kg/m^3)	x, y	Rectangular coordinates (m)
$\bar{C}$	Coefficient of viscous damping forces (Pa s/m)	**Greek symbols**	
c	constant wave speed (m/s)	ρ	Density of the fluid (kg/m^3)
D	coefficient of mass diffusion (m^2/s)	ζ	Specific heat at constant volume (J/kg K)
d	half mean width of the symmetric channel (m)	λ	Wavelength (m)
E_1	membrane tension parameter	σ	Electrical conductivity of the fluid (A/V)
E_2	mass characterizing parameter	ε	Amplitude ratio
E_3	viscous damping parameter	δ	Wave number
Ec	Eckert number	κ	Thermal conductivity (W/m K)

Content from this work may be used under the terms of the Creative Commons Attribution 3.0 licence. Any further distribution of this work must maintain attribution to the author(s) and the title of the work, journal citation and DOI.
Published under licence by IOP Publishing Ltd

M	Hartmann number	ψ	Stream function (m^2/s)
m'	non-uniformity of the channel	θ	Dimensionless temperature
$\bar{m}_1$	mass per unit area (kg/m^2)	Φ	Dimensionless concentration
n	Power law index of hyperbolic tangent fluid.	β_1	Velocity slip parameter
p	Pressure (Pa)	β_2	temperature slip parameter
Pr	Prandtl number	β_3	Species slip parameter
R	Reynolds number	$\bar{\tau}$	elastic tension in the membrane (Pa m)
Sc	Schmidt number	$\tau_{xx}, \tau_{xy}, \tau_{yy}$	extra stress tensor (Pa)
Sr	Soret number	η_∞	infinite shear rate viscosity (Pa s)
t	Time (s)	η_0	zero shear rate viscosity (Pa s)
T	Dimensional Temperature (K)	Γ	Time constant (s)

1. Introduction

The term peristalsis means clasping and compressing. The peristaltic action occurs in the form of successive waves of involuntary muscular contractions passing along the walls and forcing the contents onward. In physiological situations, the mechanism is found in esophagus, stomach, intestines, small blood vessels, fallopian tube, ureter and gut. The peristaltic mechanism has been attracting the attention of bioengineers because of its importance in living body system and in the design of biomedical instruments such as dialysis machines, open-heart bypass pump machines, artificial lungs and tissues.

Several attempts have been made by considering physiological fluids as Newtonian. A few investigations pertaining to peristaltic flow of Newtonian fluids have been reported in [1-5]. Further, some interesting results has been put forward in rheological complex physiological fluids such as blood (Power-law model, Casson model and Herschel - Bulkley model), chyme (Williamson model), bread and white eggs through esophagus (Maxwell model)and urine infection (couple-stress model) to be non-Newtonian during pumping for details, see [6-11]. Among non-Newtonian fluids, hyperbolic tangent fluid model characterize the flow behaviour of shear thinning fluids. Nadeem and Akram [12] addressed the peristaltic pumping of a hyperbolic tangent fluid through an asymmetric channel. Nadeem and Maraj [13] studied mathematically the peristaltic motion of a hyperbolic tangent fluid in a curved channel with the help of Homotopic perturbation method. Ali Abbas *et al.* [14] reported the 3D peristaltic pumping of hyperbolic tangent fluid with flexible walls.

Peristaltic flow with temperature and mass transfer effects has been exploited by many authors in order to conduct diverse investigations in biomedical and biomechanical sciences. The Biological heat transfer in a living system include thermal conduction in tissue, metabolic heat generation, burn injuries, fever, perfusion of blood flow and hyperthermia. The biological mass transfer process include glucose diffusion into the cell, absorption of proteins and peptides, liquid diffusion in tissues, drug delivery across absorption barriers. Saravana*et al.* [15] analysed mathematically the peristaltic transport of a third grade fluid through an inclined asymmetric channel by taking temperature and concentration effects into account. A few investigations on peristalsis with temperature and concentration effects have been reported in [16-18].

The influence of magnetic field may be useful to slow down the blood flow in human arterial system, controls the blood flow velocities in surgical procedures. The slip condition proposed by Navier [19] has importance in studying the flow at the fluid-wall interface and it may be more realistic model observed in gastrointestinal tract and in the flow of polymer solutions. Akram and Nadeem [20] addressed the slip effects on peristaltic motion of a hyperbolic tangent fluid model through an

asymmetric channel. Due to complex and elastic nature of physiological systems, it becomes necessary to consider the non-uniformity of the channel with wall properties. Abbas et al. [21] presented the wall properties and entropy generation for the peristaltic transport of a nanofluid in a non-uniform channel. They observed the importance of considering elastic wall parameters on the blood flow in small blood vessels. Recently, investigations are made by considering the wall properties [22-26].

In view of above, an attempt is framed to analyse the behaviour of wall properties on the peristaltic flow of a hyperbolic tangent fluid in a non-uniform channel subjected to external magnetic field, velocity and thermal slip effects. The flow is investigated in the fixed reference frame under the consideration of long wave length and low Reynolds number. Regular perturbation method has employed in the study. The influence of sundry parameters on the stream function, velocity, temperature and concentration are discussed in detail through plots.

2. Mathematical formulation of the problem

We consider the motion of an incompressible hyperbolic tangent fluid progressed by sinusoidal waves with constant wave speed 'c'. The non-uniform channel walls are assumed to be flexible and are taken as a stretched membrane. A uniform external magnetic field B_0 is applied along the y-axis. The induced magnetic field is ignored under the assumption of small magnetic Reynolds number. The thermal and the mass concentration at the lower and upper walls of channel are T_0 and C_0; T_1 and C_1, respectively and the flow geometry is illustrated in figure 1.

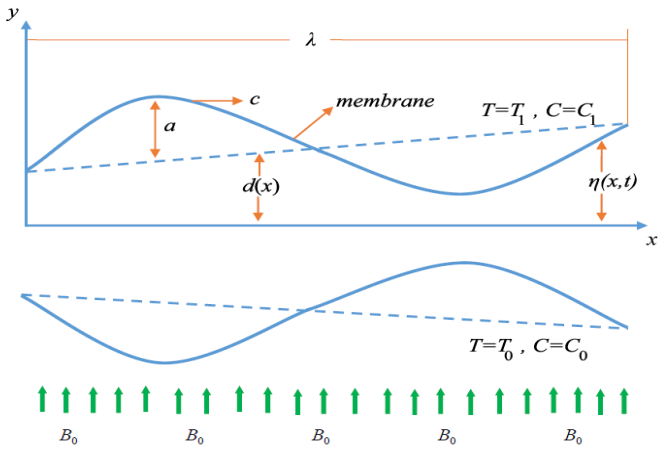

Figure 1. Physical model

The geometry of wall surface is represented by

$$y = \pm\eta(x,t) = \pm\left(d(x) + a\sin\frac{2\pi}{\lambda}(x - ct) \right) \tag{1}$$

where $d(x) = d + m'x, (m' << 1)$, a indicates amplitude, λ indicates wavelength, d is the mean width of the channel, m' indicates the dimensional channel non-uniformity and t indicates time.

The extra stress tensor in hyperbolic tangent fluid is given by

$$\tau = \left[\eta_\infty + (\eta_0 + \eta_\infty)\tanh(\Gamma\dot{\gamma})^n \right]\dot{\gamma} \tag{2}$$

and $$\dot{\gamma} = \left(\frac{1}{2}\sum_i\sum_j \dot{\gamma}_{ij}\dot{\gamma}_{ji} \right)^{1/2} = \left(\frac{1}{2}\Pi \right)^{1/2}, \tag{3}$$

where Π is the second invariant strain tensor.

For $\eta_\infty = 0$ and $\Gamma\dot{\gamma} < 1$, equation (2) can be written as

$$\tau = \eta_0 \left(\Gamma\dot{\gamma}\right)^n \dot{\gamma} = \eta_0 \left[(1+\Gamma\dot{\gamma}-1)\right]^n \dot{\gamma} = \eta_0 \left[1+n\left(\Gamma\dot{\gamma}-1\right)\right]\dot{\gamma} \tag{4}$$

The governing equations for 2D flows under the influence of magnetic field are given by

$$\frac{\partial u}{\partial x} + \frac{\partial v}{\partial y} = 0 \tag{5}$$

$$\rho\left(\frac{\partial u}{\partial t} + u\frac{\partial u}{\partial x} + v\frac{\partial u}{\partial y}\right) = -\frac{\partial p}{\partial x} + \frac{\partial \tau_{xx}}{\partial x} + \frac{\partial \tau_{xy}}{\partial y} - \sigma B_0^2 u \tag{6}$$

$$\rho\left(\frac{\partial v}{\partial t} + u\frac{\partial v}{\partial x} + v\frac{\partial v}{\partial y}\right) = -\frac{\partial p}{\partial y} + \frac{\partial \tau_{xy}}{\partial x} + \frac{\partial \tau_{yy}}{\partial y} \tag{7}$$

$$\zeta\rho\left(\frac{\partial T}{\partial t} + u\frac{\partial T}{\partial x} + v\frac{\partial T}{\partial y}\right) = \kappa\left(\frac{\partial^2 T}{\partial x^2} + \frac{\partial^2 T}{\partial y^2}\right) + \tau_{xx}\frac{\partial u}{\partial x} + \tau_{yy}\frac{\partial v}{\partial y} + \tau_{xy}\left(\frac{\partial v}{\partial x} + \frac{\partial u}{\partial y}\right) \tag{8}$$

$$\left(\frac{\partial C}{\partial t} + u\frac{\partial C}{\partial x} + v\frac{\partial C}{\partial y}\right) = D\left(\frac{\partial^2 C}{\partial x^2} + \frac{\partial^2 C}{\partial y^2}\right) + \frac{DK_T}{T_m}\left(\frac{\partial^2 T}{\partial x^2} + \frac{\partial^2 T}{\partial y^2}\right) \tag{9}$$

where K_T and T_m indicates the thermal diffusion ratio and the mean temperature.

The equation governing the flexible wall motion is expressed as $L^*(\eta) = p - p_0$ (10)

where L^* is an operator such that $L^* = -\bar{\tau}\frac{\partial^2}{\partial x^2} + \bar{m}_1\frac{\partial^2}{\partial t^2} + \bar{C}\frac{\partial}{\partial t}$ (11)

Here p_0 is the outside surface pressure on the wall due to the tension and we choose that $p_0 = 0$.

The fluid-wall interface boundary conditions with velocity slip, thermal and concentration jump conditions are given by

$$u \pm \beta_1 \tau_{xy} = 0,\ T \pm \beta_2 \frac{\partial T}{\partial y} = \begin{bmatrix} T_1 \\ T_0 \end{bmatrix},\ C \pm \beta_3 \frac{\partial C}{\partial y} = \begin{bmatrix} C_1 \\ C_0 \end{bmatrix} \text{ at } y = \pm\eta \tag{12}$$

and the wall flexibility dynamic boundary are

$$\frac{\partial}{\partial x}L^*(\eta) = \frac{\partial p}{\partial x} = \frac{\partial \tau_{xx}}{\partial x} + \frac{\partial \tau_{xy}}{\partial y} - \sigma B_0^2 u - \rho\left(\frac{\partial u}{\partial t} + u\frac{\partial u}{\partial x} + v\frac{\partial u}{\partial y}\right) \tag{13}$$

The stream function $\psi(x, y, t)$ such that

$$u = \frac{\partial \psi}{\partial y},\ v = -\frac{\partial \psi}{\partial x}. \tag{14}$$

The dimensionless quantities are given below:

$$x' = \frac{x}{\lambda},\ y' = \frac{y}{d},\ \psi' = \frac{\psi}{cd},\ t' = \frac{ct}{\lambda},\ p' = \frac{d^2}{c\lambda\eta_0}p,\ \dot{\gamma}' = \frac{\dot{\gamma}d}{c},\ \eta' = \frac{\eta}{d},\ \tau'_{xx} = \frac{\lambda}{\eta_0 c}\tau_{xx},\ \tau'_{xy} = \frac{d}{\eta_0 c}\tau_{xy},$$

$$\tau'_{yy} = \frac{d}{\eta_0 c}\tau_{yy},\ R = \frac{\rho cd}{\eta_0},\ \varepsilon = \frac{a}{d},\ \delta = \frac{d}{\lambda},\ m = \frac{m'\lambda}{d},\ We = \frac{\Gamma c}{d},\ M = \sqrt{\frac{\sigma}{\eta_0}}B_0 d,\ Ec = \frac{c^2}{\zeta\left(T_1 - T_0\right)},$$

$$\theta=\frac{(T-T_0)}{(T_1-T_0)},\ \Phi=\frac{(C-C_0)}{(C_1-C_0)},\ \beta_1'=\frac{\beta_1}{d},\ \beta_2'=\frac{\beta_2}{d},\ \beta_3'=\frac{\beta_3}{d},\ Sc=\frac{\eta_0}{\rho D},\ Sr=\frac{\rho D K_T(T_1-T_0)}{\eta_0 T_m(C_1-C_0)},$$
$$E_1=\frac{-\bar{\tau}d^3}{\lambda^3\eta_0 c},\ E_2=\frac{\bar{m}_1 c d^3}{\lambda^3\eta_0},\ E_3=\frac{\bar{C}d^3}{\lambda^2\eta_0} \tag{15}$$

With the above dimensionless quantities, equations (5)-(9) and boundary conditions (12) and (13) along with the long wavelength and low Reynolds numberassumptions, (after dropping the primes) become

$$\frac{\partial p}{\partial x}=\frac{\partial \tau_{xy}}{\partial y}-M^2\frac{\partial \psi}{\partial y} \tag{16}$$

$$\frac{\partial p}{\partial y}=0 \tag{17}$$

$$\frac{\partial^2\theta}{\partial y^2}+Br\,\tau_{xy}\left(\frac{\partial^2\psi}{\partial y^2}\right)=0 \tag{18}$$

$$\frac{1}{Sc}\left(\frac{\partial^2\Phi}{\partial y^2}\right)+Sr\left(\frac{\partial^2\theta}{\partial y^2}\right)=0 \tag{19}$$

$$\frac{\partial\psi}{\partial y}\pm\beta_1\tau_{xy}=0,\ \theta\pm\beta_2\frac{\partial\theta}{\partial y}=\begin{bmatrix}1\\0\end{bmatrix},\ \Phi\pm\beta_3\frac{\partial\Phi}{\partial y}=\begin{bmatrix}1\\0\end{bmatrix}\text{ at } y=\pm\eta \tag{20}$$

$$\frac{\partial\tau_{xy}}{\partial y}-M^2\frac{\partial\psi}{\partial y}=\left[E_1\frac{\partial^3}{\partial x^3}+E_2\frac{\partial^3}{\partial x\partial t^2}+E_3\frac{\partial^2}{\partial x\partial t}\right](\eta) \tag{21}$$

where $\tau_{xy}=(1-n)\frac{\partial^2\psi}{\partial y^2}+nWe\left(\frac{\partial^2\psi}{\partial y^2}\right)^2$ and $Br=Ec.\Pr$ (Brinkman number).

Equation (17) indicates that $p\neq p(y)$.

Eliminating p from equations (16) and (17), we get

$$\frac{\partial^2}{\partial y^2}\left[\frac{\partial^2\psi}{\partial y^2}+\frac{n}{(1-n)}We\left(\frac{\partial^2\psi}{\partial y^2}\right)^2\right]-\frac{M^2}{(1-n)}\frac{\partial^2\psi}{\partial y^2}=0 \tag{22}$$

3. Solution of the problem

The equation (16) is not a linear and its exact solution is not possible. Hence we utilise the perturbation technique with small Weissenberg number in the form of

$$\left.\begin{aligned}\psi&=\psi_0+We\,\psi_1+O(We^2)\\ \theta&=\theta_0+We\,\theta_1+O(We^2)\\ Z&=Z_0+We\,Z_1+O(We^2)\\ \Phi&=\Phi_0+We\,\Phi_1+O(We^2)\end{aligned}\right\} \tag{23}$$

By using equation (23) the Perturbation solution satisfying the fluid-wall boundary conditions are given by

$$\psi = A_0\left[\frac{\sinh ry}{rS_1} - y\right] + We\frac{A_0^2 n(\cosh ry - 1)}{6(n-1)S_1^2 S_2}\begin{pmatrix} 2\sinh r\eta(1+\cosh ry - S_3) \\ +(1-n)r\beta_1(S_3(1+\cosh ry) - S_4 - 3)\end{pmatrix}, \tag{24}$$

$$u = A_0\left[\frac{\cosh ry}{S_1} - 1\right] + We\frac{A_0^2 nr\sinh ry}{6(n-1)S_1^2 S_2}\begin{pmatrix} 2\sinh r\eta(2\cosh ry - S_3) \\ +(n-1)r\beta_1(3 - 2S_3\cosh ry + S_4)\end{pmatrix}, \tag{25}$$

$$\theta = \frac{Br(1-n)A_0^2}{8S_1^2}\left(\cosh 2r\eta - \cosh 2ry - 2r^2(\eta^2 - y^2) + 2r\beta_2(\sinh 2r\eta - 2r\eta)\right) + \frac{1}{2}\left(1 + \frac{y}{(\eta+\beta_2)}\right)$$
$$+ We\begin{pmatrix} \frac{A_0^3 rBr\,n}{432S_1^3 S_2(\eta+\beta_2)}(S_5 + 6r\beta_2 S_7 + (n-1)r\beta_1(S_8 + 12r\beta_2 S_9))\,y \\ +\frac{2A_0^3 rBr\,n\sinh ry}{432S_1^3 S_2}(4((7+5\cosh 2ry)\sinh r\eta + 9S_6\cosh ry)) \\ +\left(\frac{2A_0^3 Br\,n(n-1)r^2\beta_1\sinh ry}{432S_1^3 S_2}\right)(\cosh ry(54+18S_4) - S_3(10\cosh 2ry + 14))\end{pmatrix} \tag{26}$$

$$\Phi = \frac{-A_0^2 Br(1-n)ScSr}{8S_1^2}\left[S_4 + 2r\beta_3(S_6 - 2r\eta) - \cosh 2ry - 2r^2(\eta^2 - y^2)\right] + \frac{1}{2}\left(1 + \frac{y}{(\eta+\beta_3)}\right)$$
$$+ We\begin{pmatrix} \frac{-A_0^3 r\,Br\,Sc\,Sr\,n}{432S_1^3 S_2(\eta+\beta_3)}(S_5 + 6r\beta_3 S_7 + (n-1)r\beta_1(S_8 + 12r\beta_3 S_9)) \\ -\frac{2A_0^3\,r\,Br\,Sc\,Sr\,n\sinh ry}{432S_1^3 S_2}(4((7+5\cosh 2ry)\sinh r\eta + 9S_6\cosh ry)) \\ -\frac{2A_0^3 Br\,Sc\,Sr\,n(n-1)r^2\beta_1\sinh ry}{432S_1^3 S_2}(\cosh ry(54+18S_4) - S_3(10\cosh 2ry + 14))\end{pmatrix} \tag{27}$$

$$Z = \eta_x\left.\frac{\partial\theta_0}{\partial y}\right|_{y=\eta} + We\eta_x\left.\frac{\partial\theta_1}{\partial y}\right|_{y=\eta} \tag{28}$$

$$= \eta_x\left[\frac{1}{2(\eta+\beta_2)} + \frac{A_0^2 Br(1-n)r}{4S_1^2}(2r\eta - S_6)\right]$$
$$- We\eta_x\frac{A_0^3 rBrn}{432S_1^3 S_2(\eta+\beta_2)}\begin{pmatrix} -36 + 8S_4 + 28\cosh 4r\eta + 12r\eta S_6 - 66r\eta\sinh 4r\eta \\ +(n-1)r\beta_1(-60r\eta S_4 + 12r\eta\cosh 4r\eta + 26S_6)\end{pmatrix} \tag{29}$$

where

$$r^2 = \frac{M^2}{1-n};\ A_0 = \frac{8\varepsilon\pi^3}{r^2(1-n)}\left[\frac{E_3}{2\pi}\sin 2\pi(x-t) - (E_1+E_2)\cos 2\pi(x-t)\right];$$

$S_1 = \cosh r\eta + (1-n)r\beta_1\sinh r\eta$; $S_2 = \sinh r\eta + (1-n)r\beta_1\cosh r\eta$; $S_3 = 2\cosh r\eta$; $S_4 = \cosh 2r\eta$;
$S_5 = -16(8+7S_4)\sinh^2 r\eta$; $S_6 = \sinh 2r\eta$; $S_7 = 2S_6 - 11\sinh 4r\eta$; $S_8 = -26S_6 + \sinh 4r\eta$;
$S_9 = \cosh 4r\eta - 5S_4$;

4. Results and Discussion

4.1.Velocity profiles

The velocity expression is given in the equation (25). The velocity distributions are graphically presented in figures (2)-(7) to analyse the effect of velocity slip parameter β_1, hyperbolic power law

index n, Weissenberg number We, Hartmann number M, non-uniform parameter m, membrane tension parameter E_1, mass characterizing parameter E_2 and the viscous damping parameter E_3 with $x=0.2$ and $t=0.1$. Figure 2 is illustrated to study the effect of β_1 on the distribution of velocity *u*. It is clear that the velocity of the fluid increases with increasing the velocity slip. From figure 3, we observe that the velocity increases with enhancing the power law index n of a hyperbolic tangent fluid.

Figure 4 shows that the velocity of the hyperbolic tangent fluid increases with increasing We in the upper half of the channel butthe behaviour is opposite in the lower half of the channel. Figure 5 depicts that the distribution of velocity decreases with an increase in M. As expected fromfigure 6, we find that the flow characteristics for a divergent channel $(m>0)$is high compared to uniform channel $(m=0)$ and is low for a convergent channel$(m<0)$. In figure 7, we observe that the velocity profile increases with increasing E_1 and E_2; and decreases with increasing E_3.

4.2 Temperature profiles

The equation (26) shows the temperature expression.Temperature distributions are plotted in figures 8-13 to study the effects of the thermal slip parameter β_2, $\beta_1, M, We, n, E_1, E_2$ and E_3 with $x=0.2$ and $t=0.1$.Figure 8 and figure 9 are drawn to study the effect of β_2 and β_1 on the temperature distribution θ. We see that the temperature increases with increasing β_2 and decreases with increasing β_1. From figure 10, we observe that the temperature decreases with increasing *M*. In figure 11, we find that the temperature distribution increases with increasing We in the upper half of the channel, whereas it has opposite behaviour in the lower half of the channel. Figure 12 shows that an increase in power law index *n* increases the temperature. Figure 13 shows that the temperature increases with increasing E_1 and E_2; and it decreases with increasing E_3.

4.3 Concentration profiles

The equation (27) shows for the concentration field expression.The influence of the concentration slip parameter β_3, Schmidt number Sc, Soret number Sr, β_1 and n on the concentration profileswith $x=0.2$ and $t=0.1$are shown graphically in figures 14-18. From figure 14, we notice that the concentrationdistribution decreases with increasing β_3. Figures 15 and 16 illustrates that the concertation decreases with increasing Schmidt number and Soret number. In Figure 17 and figure 18, we seen that the mass concentration increases by increasing β_1 and the mass concentration decreases by increasing n.

4.4 Coefficient of heat transfer profiles

The equation (29) gives the coefficient of heat transfer expression at the wall. Figures from (19)-(23) are plotted to study the variation of thermal transfer coefficient at the flexible wall. We notice that the nature the thermal transfer is oscillatory because of oscillatory nature of the wall. From the figures 19, 20, 21 and 23, the magnitude of thermal transfer coefficient decreases by increasing β_1, n, M and E_3; and from figures 22 and 23, it increases by increasing Br, E_1 and E_2.

4.5. Stream line patterns

From equation (24) we have calculated the stream function in terms of *y* and figure 24 shows the stream line behaviour of power law index of hyperbolic tangent fluid. We found that the volume of trapping bolus increases with an increase of n. From figures 25 and 26, it is found that the size of the trapping bolus increases with increasing β_1 and We. Figure 27 depicts that the size of the trapped bolus decreases by increasing *M*.

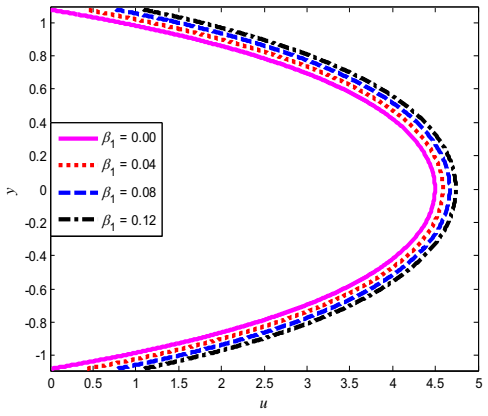

Figure 2. Distribution of u with y for different values of β_1 with $E_1=0.6$, $E_2=0.6$, $E_3=0.4$, $\varepsilon=0.1, M=2, m=0.1, We=0.01$, $n=0.02$.

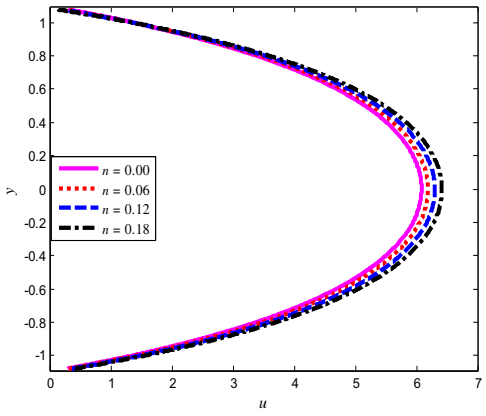

Figure 3. Distribution of u with y for different values of n with $E_1=0.8$, $E_2=0.8$, $E_3=0.4$, $\varepsilon=0.1, \beta_1=0.02, m=0.1$, $M=2$, $We=0.04$.

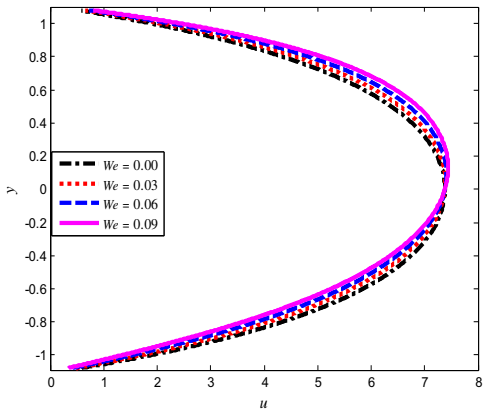

Figure 4. Distribution of u with y for different values of We with $E_1=1$, $E_2=0.8$, $E_3=0.4$, $\varepsilon=0.1, \beta_1=0.04, m=0.1$, $M=2$, $n=0.04$.

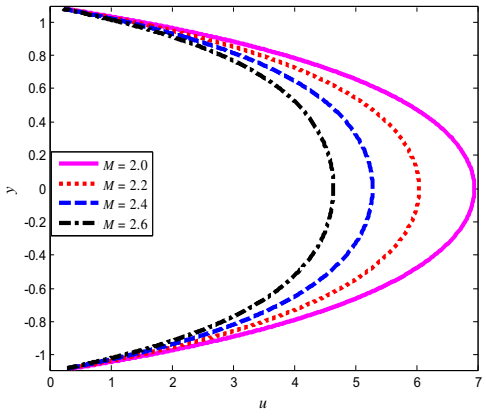

Figure 5. Distribution of u with y for different values of M with $E_1=1$, $E_2=0.8$, $E_3=0.4$, $\varepsilon=0.1, \beta_1=0.02, m=0.1$, $We=0.01, n=0.04$.

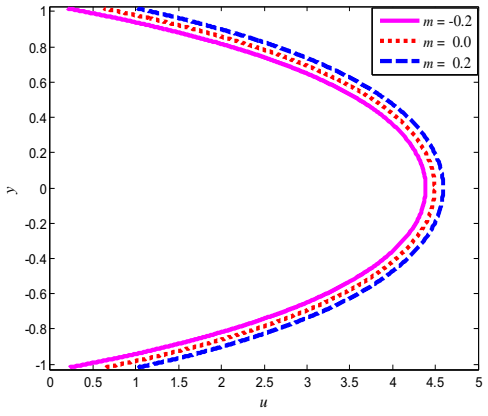

Figure 6. Distribution of u with y for different values of m with $E_1=0.6$, $E_2=0.6$, $E_3=0.4$, $\varepsilon=0.1, M=2$, $\beta_1=0.02, We=0.04, n=0.02$.

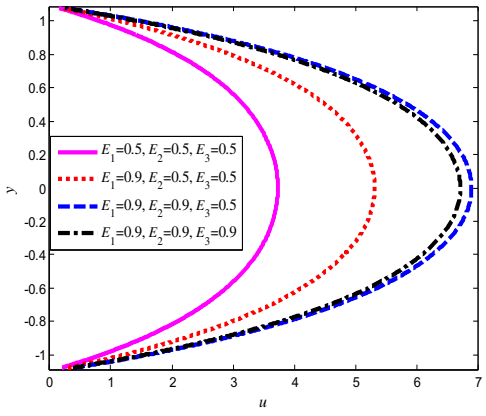

Figure 7. Distribution of u with y for different values of E_1, E_2, E_3 with $\varepsilon=0.1$, $\beta_1=0.02$, $m=0.1, n=0.04$, $M=2$, $We=0.01$.

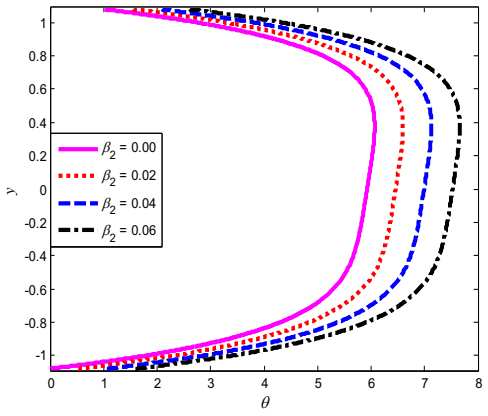

Figure 8. Temperature profiles for β_2 with $E_1 = 0.6$, $E_2 = 0.6$, $E_3 = 0.4$, $\varepsilon = 0.1$, $\beta_1 = 0.02$, $n = 0.02$, $M = 2$, $m = 0.1$, $We = 0.01$, $Br = 1$.

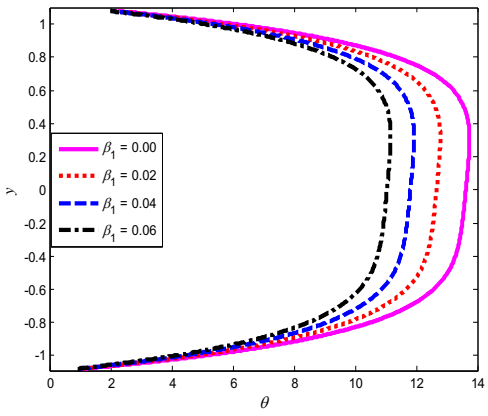

Figure 9. Temperature profiles for β_1 with $E_1 = 0.6$, $E_2 = 0.6$, $E_3 = 0.4$, $\varepsilon = 0.1$, $M = 2$, $\beta_2 = 0.02$, $We = 0.01$, $n = 0.02$, $m = 0.1$, $Br = 2$

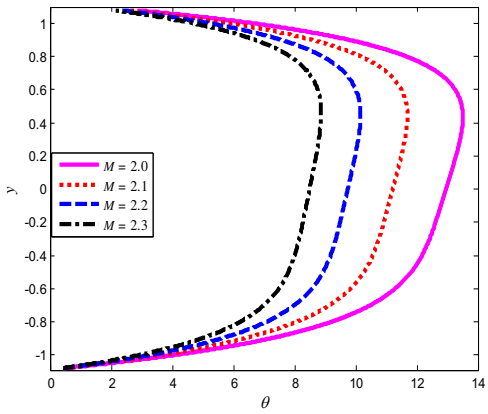

Figure 10. Temperature profiles for M with $E_1 = 0.6$, $E_2 = 0.6$, $E_3 = 0.4$, $\varepsilon = 0.1$, $\beta_1 = 0.02$, $\beta_2 = 0.02$, $We = 0.06$, $n = 0.02$, $m = 0.1$, $Br = 2$.

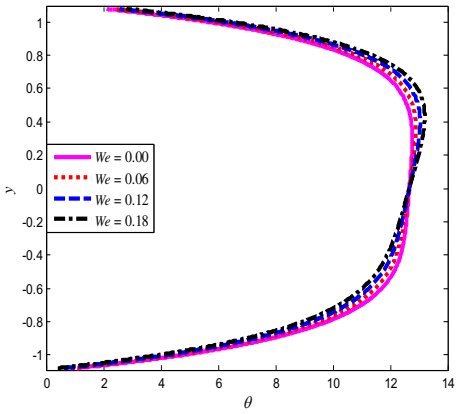

Figure 11. Temperature profiles for We with $E_1 = 0.6$, $E_2 = 0.6$, $E_3 = 0.4$, $\varepsilon = 0.1$, $\beta_1 = 0.02$, $\beta_2 = 0.02$, $M = 2$, $n = 0.02$, $m = 0.1$, $Br = 2$.

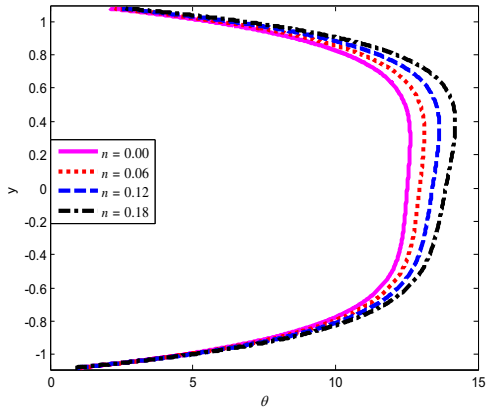

Figure 12. Temperature profiles for n with $E_1 = 0.6$, $E_2 = 0.6$, $E_3 = 0.4$, $\varepsilon = 0.1$, $\beta_1 = 0.02$, $\beta_2 = 0.02$, $M = 2$, $We = 0.01$, $m = 0.1$, $Br = 2$.

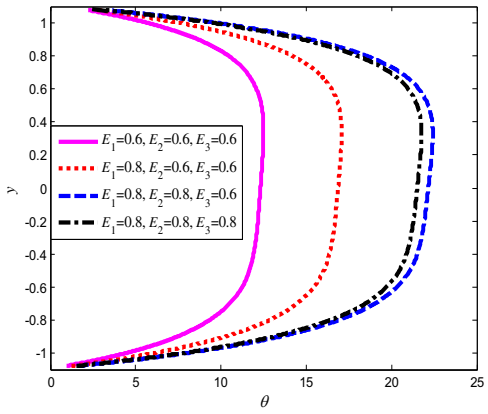

Figure 13. Temperature profiles for E_1, E_2 and E_3 with $\varepsilon = 0.1$, $\beta_1 = 0.02$, $\beta_2 = 0.02$, $We = 0.06$, $M = 2$, $n = 0.02$, $m = 0.1$, $Br = 2$.

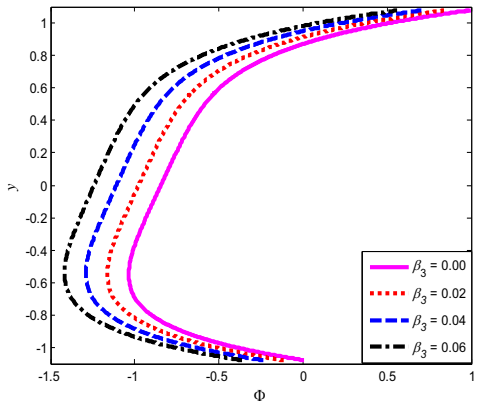

Figure 14. Concentration profiles for β_3 with $E_1 = 0.6$, $E_2 = 0.6$, $E_3 = 0.4$, $\varepsilon = 0.1$, $\beta_1 = 0.02$, $We = 0.01$, $m = 0.1$, $M = 2$, $n = 0.04$, $Br = 1.2$, $Sc = 0.2$, $Sr = 1$.

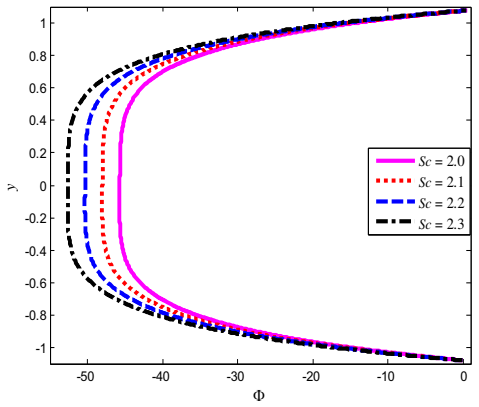

Figure 15. Concentration profiles for Sc with $E_1 = 0.6$, $E_2 = 0.6$, $E_3 = 0.4$, $\varepsilon = 0.1$, $\beta_1 = 0.01$, $\beta_3 = 0.02$, $We = 0.01$, $m = 0.1$, $M = 2$, $n = 0.02$, $Br = 2$, $Sr = 2$.

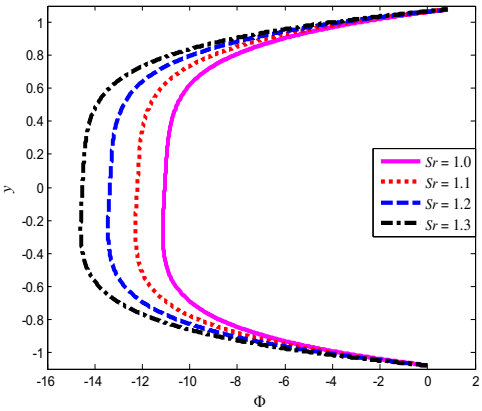

Figure 16. Concentration profiles for Sr with $E_1 = 0.6$, $E_2 = 0.6$, $E_3 = 0.4$, $\varepsilon = 0.1$, $\beta_1 = 0.01$, $\beta_3 = 0.02$, $We = 0.01$, $m = 0.1$, $M = 2$, $n = 0.02$, $Br = 2$, $Sc = 0.2$.

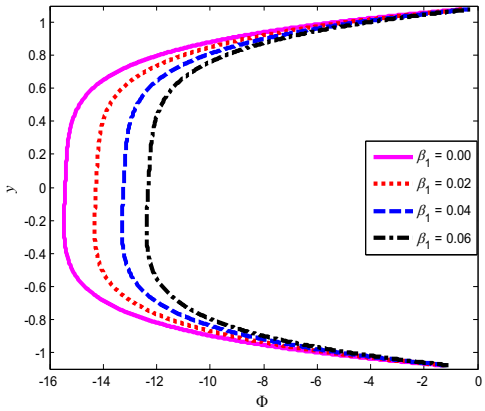

Figure 17. Concentration profiles for β_1 with $E_1 = 0.6$, $E_2 = 0.6$, $E_3 = 0.4$, $\varepsilon = 0.1$, $\beta_3 = 0.02$, $We = 0.01$, $m = 0.1$, $M = 2$, $n = 0.04$, $Br = 1.2$, $Sc = 0.2$, $Sr = 2$.

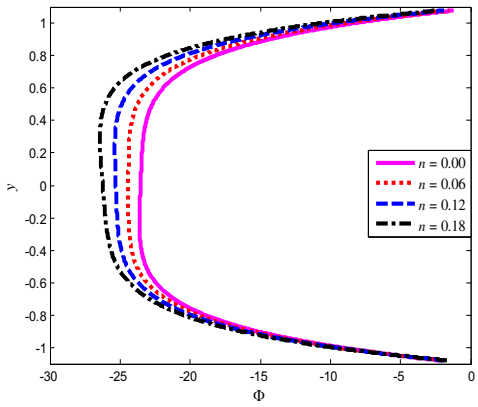

Figure 18. Concentration profiles for n with $E_1 = 0.6$, $E_2 = 0.6$, $E_3 = 0.4$, $\varepsilon = 0.1$, $\beta_1 = 0.01$, $\beta_3 = 0.02$, $We = 0.02$, $m = 0.1$, $M = 2$, $Br = 2$, $Sc = 1$, $Sr = 2$.

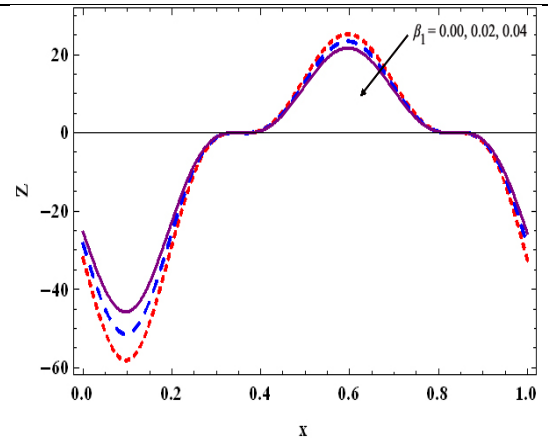

Figure 19. Distribution of Z with x for different values of β_1 with $E_1=1$, $E_2=0.6$, $E_3=0.4$, $\varepsilon=0.1$, $m=0.1, We=0.04, Br=2, \beta_2=0.02$, $M=3$, $n=0.02$, $t=0.1$.

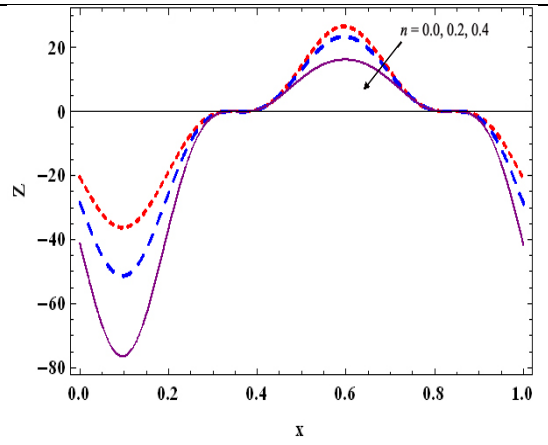

Figure 20. Distribution of Z with x for different values of n with $E_1=1$, $E_2=0.6$, $E_3=0.4$, $\varepsilon=0.1$, $m=0.1, We=0.04$, $Br=2$, $\beta_2=0.02$, $M=3$, $\beta_1=0.02$, $t=0.1$.

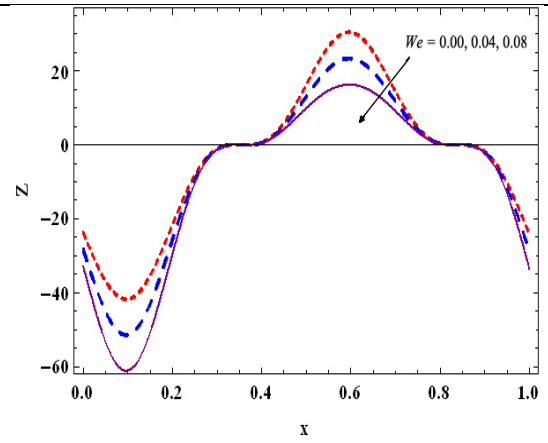

Figure 21. Distribution of Z with x for different values of We with $E_1=1$, $E_2=0.6$, $E_3=0.4$, $\varepsilon=0.1$, $m=0.1, \beta_1=0.02$, $Br=2$, $\beta_2=0.02$, $M=3$, $n=0.2$, $t=0.1$.

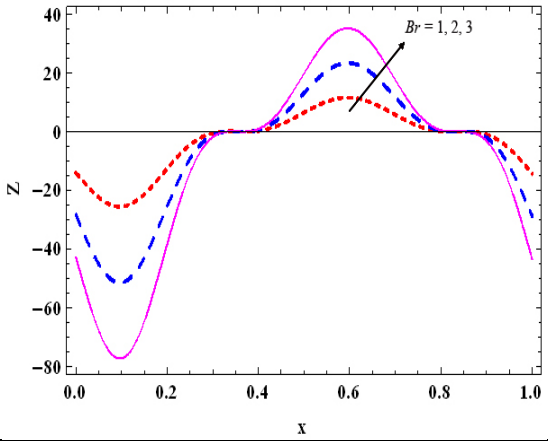

Figure 22. Distribution of Z with x for different values of Br with $E_1=1$, $E_2=0.6$, $E_3=0.4$, $\varepsilon=0.1, m=0.1, We=0.04, \beta_1=0.02$, $\beta_2=0.02$, $M=3$, $n=0.2$, $t=0.1$.

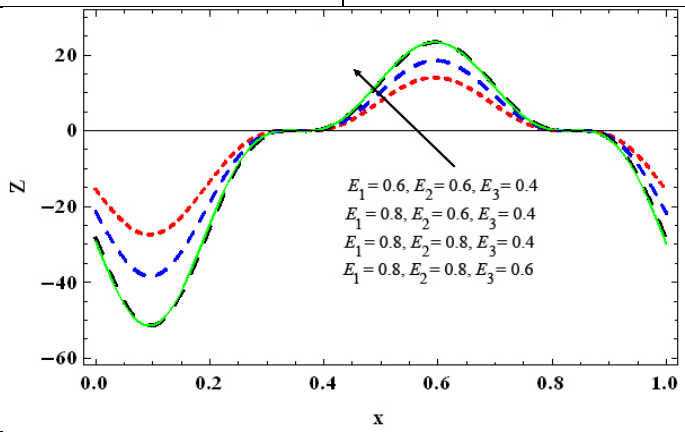

Figure 23. Distribution of Z with x for different values of E_1, E_2 and E_3 with $\varepsilon=0.1$, $m=0.1$, $We=0.04$ $\beta_1=0.02$, $\beta_2=0.02$, $M=3$, $n=0.2$, $Br=2$, $t=0.1$.

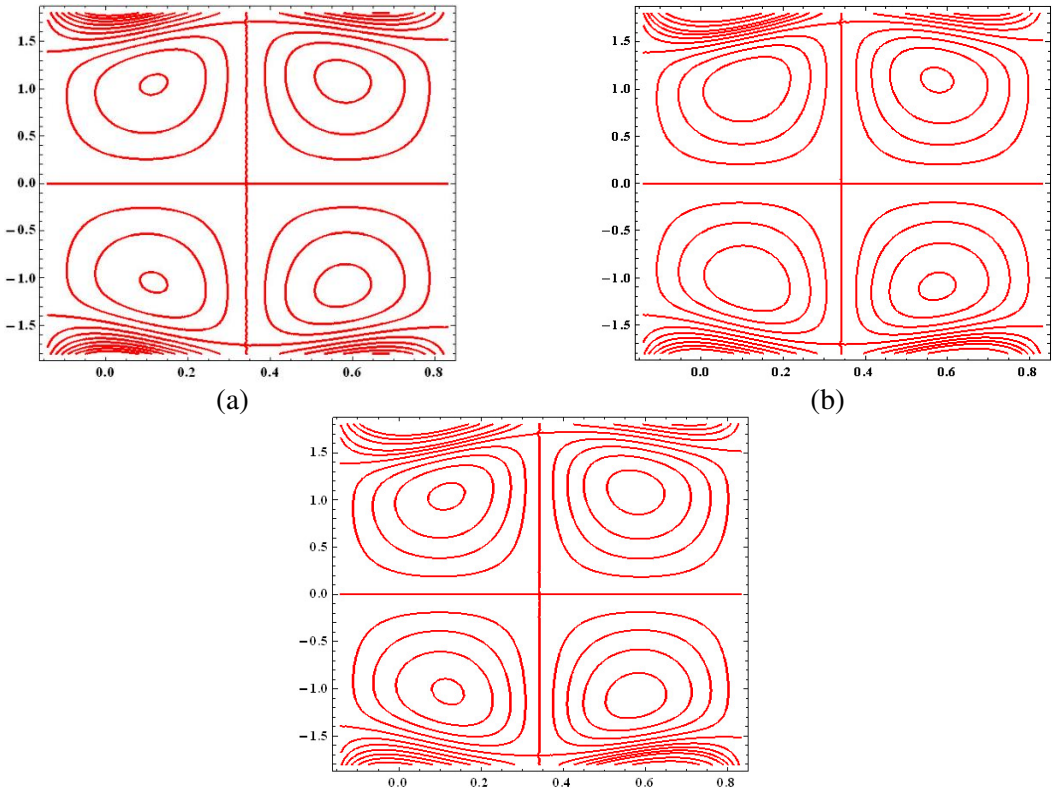

Figure 24. Streamlines for (a) $n=0.00$ (b) $n=0.01$ (c) $n=0.02$ with $E_1=0.6$, $E_2=0.6$, $E_3=0.4$, $\beta_1=0.03$, $We=0.04$, $\varepsilon=0.1$, $m=0.1$, $M=3$, $t=0.1$

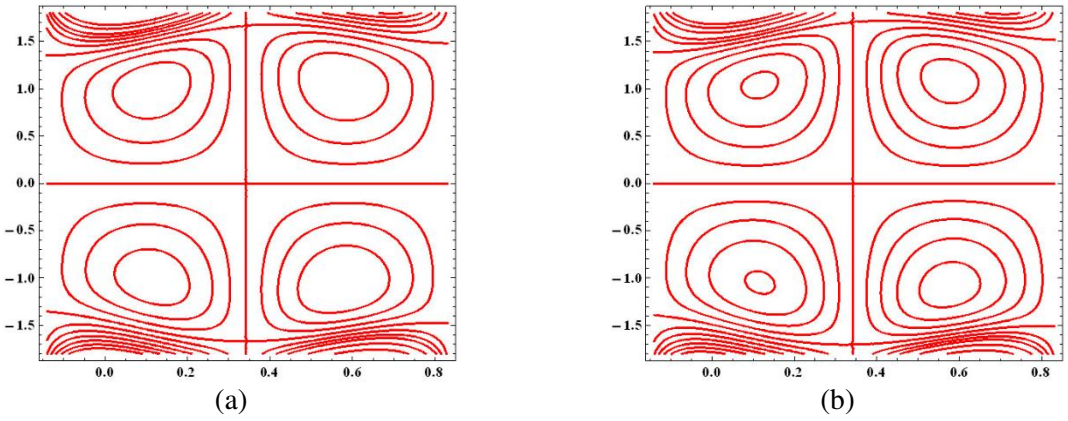

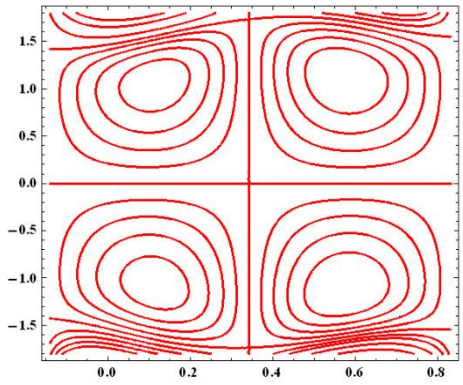

(c)

Figure 25. Streamlines for (a) $\beta_1 = 0.00$ (b) $\beta_1 = 0.03$ (c) $\beta_1 = 0.06$ with $E_1 = 0.6$, $E_2 = 0.6$, $E_3 = 0.4, \varepsilon = 0.1$, $m = 0.1, We = 0.04$, $M = 3$, $n = 0.02$, $t = 0.1$.

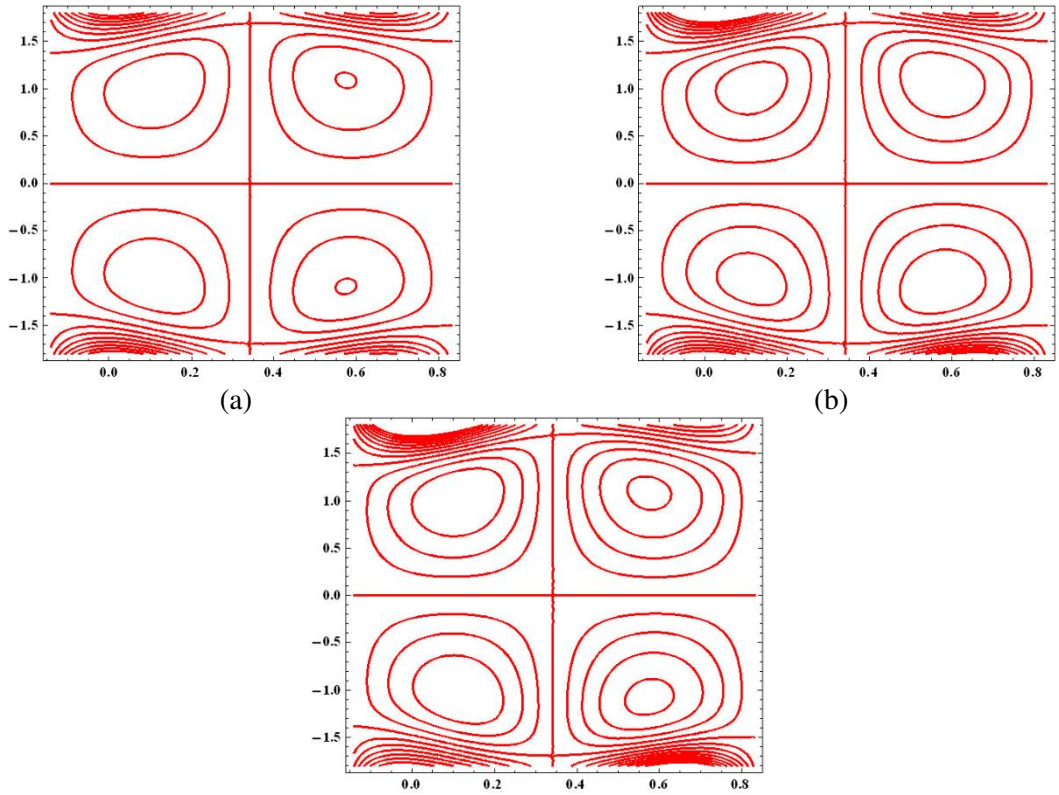

(a) (b)

(c)

Figure 26. Streamlines for (a) $We = 0.00$ (b) $We = 0.02$ (c) $We = 0.04$ with $E_1 = 0.6$, $E_2 = 0.6$, $E_3 = 0.4, \beta_1 = 0.02$, $\varepsilon = 0.1$, $m = 0.1, M = 3$, $n = 0.02$, $t = 0.1$.

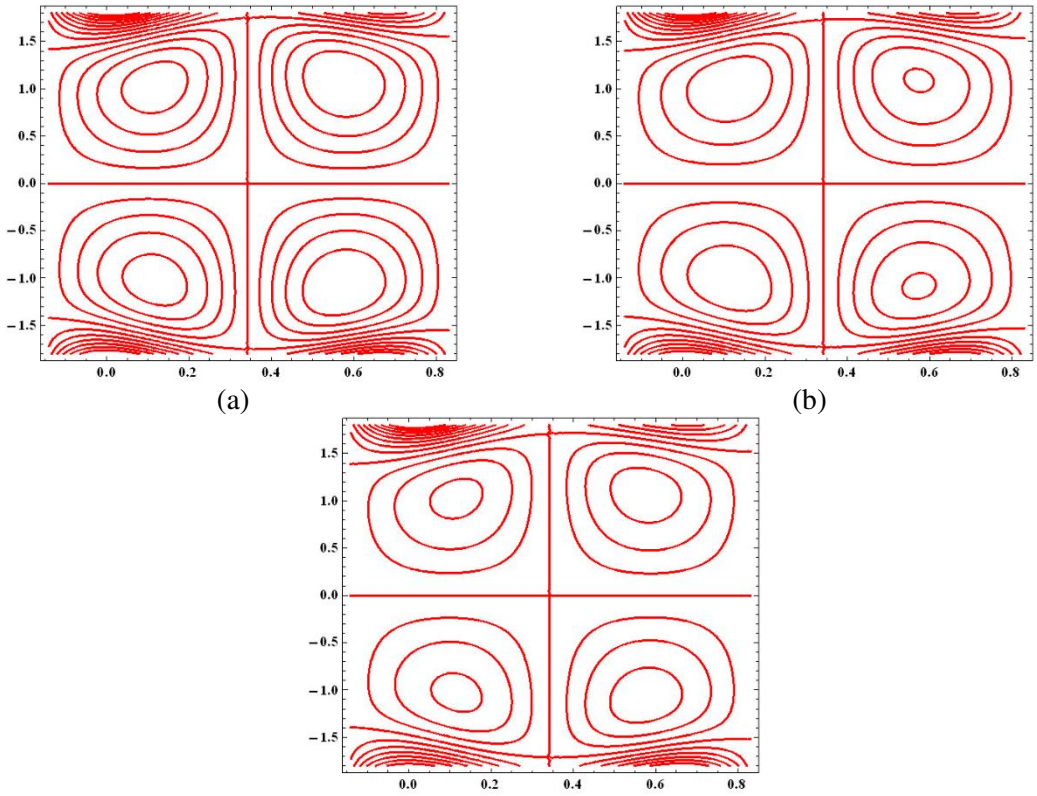

Figure 27. Streamlines for (a) $M=2.4$, (b) $M=2.6$ (c) $M=2.8$ with $E_1=0.6$, $E_2=0.6$, $E_3=0.4$, $\beta_1=0.02$, $\varepsilon=0.1$, $m=0.1$, $We=0.02$, $n=0.02$, $t=0.1$.

5. Conclusions

In this paper, we study the combined effects of velocity slip conditions, temperature, concentration jump boundary conditions and wall properties on MHD peristaltic transport of a hyperbolic tangent fluid in a non-uniform channel under the assumptions of long wavelength and low Reynolds number. The perturbation solutions in terms of small Weissenberg number are obtained for the stream function, velocity, temperature, concentration and the coefficient of heat transfer. The effect of various parameters on the flow characteristics are presented graphically and discussed. The main observations of this study are as follows:

- The velocity increases with the increasing the velocity slip parameter.
- The velocity and temperature increases with increasing the power law index of a hyperbolic tangent fluid whereas the concentration decreases with increasing n.
- The velocity profile increases with an increasing the Weissenberg number in the upper half of the channel whereas it decreases in the lower half of the channel.
- The heat transfer coefficient is oscillatory in nature.
- The size of trapped bolus increases with the increase of power law index n.
- The results of no slip conditions can be deduced from the analysis when $\beta_1=0, \beta_2=0$ and $\beta_3=0$.

References

[1] ShapiroA H, JaffrinMY and WeinbergSL 1969*J. Fluid Mech.***37** 799-825.
[2] Jaffrin M Y and ShapiroA H 1971*Ann. Rev. Fluid Mech.***3** 13-36.
[3] Mittra T Kand Prasad S N 1973*J Biomech.***6** 681-93.

[4] Shukla J B, Parihar R S, RaoBRP and Gupta S P 1980*J. Fluid Mech.***97** 225-37.
[5] Mishra M and Ramachandra Rao A 2003*Z. Angew. Math. Phys.***54** 532-50.
[6] Raju K K and Devanathan R 1972*Rheol. Acta***11** 170-8.
[7] Srivastava L M and Srivastava V P1984 *J Biomech.* **17(11)**821-9.
[8] Vajravelu K, Sreenadh, S and Ramesh Babu V 2005*Int. J. Non-linear Mech.***40** 83-90.
[9] Nadeem S, Ashiq S and Ali M 2012*Math. Probl. Eng.* 1-18 DOI:10.1155/2012/479087.
[10] Pandey S K and Tripathi D 2012*Appl. Math. Mech. Engl,***33(1)** 15–24.
[11] ShehaweyEL E F and MekheimerKh. S 1994 *J Phys D Appl. Phys.***27**1163-70.
[12] Nadeem S and Akram S 2009 *Z. Naturforsch***64a**559–567.
[13] Nadeem S and Maraj M N 2013*Commun. Theor. Phys,***59(6)** 729-36.
[14] Ali Abbas M, Bai Y Q, Bhatti M M and Rashidi M M 2016*AEJ***55(1)** 653-62.
[15] Saravana R, Hemadri Reddy R, Sreenadh S, Venkataramana S and Kavitha A 2013 *Int. J. of Appl. Math and Mech.***9(11)** 51-86.
[16] Nadeem S and Noreen Sher Akbar 2010*Commun Nonlinear Sci Numerical Simul***15** 2860 – 77.
[17] Akbar N S and Nadeem S 2011*Int. J. Numer. Meth. Fl.***67(12)** 1818-32.
[18] Hayat T, Hina S and Hendi, AA 2011*Chinese Phys. Lett.***28(8)** 084707(1– 4).
[19] NavierC LM 1827*Mem. Acad. R. Sci. Inst. Fr.***6**389-440.
[20] Akram S and Nadeem S 2015*Comput. Math. Math. Phys*+**55(11)**1899-1912.
[21] Abbas M A, Bai Y, Rashidi M M and Bhatti M M. 2016 *Entropy***18**
[22] Vajravelu K, Sreenadh S and Saravana R 2013*Appl. Math. Comput.***225**656-76.
[23] Srinivas S andKothandapani M 2009*Appl. Math. Comput.***213** 197-208.
[24] Hayat T, Hina S and Hendi A A 2011*Heat Transfer-Asian Research***40(7)** 577-92.
[25] Hayat T, Hina S, Hendi A A and Asghar S 2012*Int. J. Heat Mass Tran.***54** 3511-21.
[26] Saravana R, Sreenadh S, Venkataramana S, Hemadri Reddy R andKavitha A 2011*IJICTE***1(11)** 10-24.